Supplementary Materials for "Computational Model Predicts Paracrine and Intracellular Drivers of Fibroblast Phenotype After Myocardial Infarction"

Supplementary Methods

Alterations to the original network structure

Additions were made to the original fibroblast signaling network model [1] to make predictions more comprehensive of fibroblast phenotype and its effect on the extracellular matrix (see **Figure S1**). Specifically, we introduced three new nodes into the network: LOX, x-linked fibers (cross-linked collagen fibers), and contraction. The new reactions were supported by at least two published studies that used rat or human fibroblasts - the same criteria used in the initial development of the model network [1], with literature sources provided in **Table S1** [2–9]. Additionally, we separated the nodes that represent the levels of the exogenous paracrine inputs to the model from the nodes that represent the paracrine signals available to bind to each receptor, as indicated by the green nodes at the top of the network on **Figure S1**. This allowed the exogenous paracrine signals to be defined in a time-dependent manner as described below, while still modeling the autocrine behavior of some signaling inputs such as AngII.

Logic-based differential equation modeling framework

The form of the logic-based differential equations used to model these interactions are the same as those used in the original model. Activation is modeled using a normalized saturating Hill function where $f_{act}(x=0) = 0$, $f_{act}(x=EC50) = 0.5$, and $f_{act}(x=1)=1$. Inhibition is modeled using a a normalized saturating Hill function where $f_{inhib}(x=0) = 1$, $f_{inhib}(x=EC50) = 0.5$, and $f_{inhib}(x=1)=0$. Crosstalk between pathways is modeled using logical AND ("f(x)*f(y)") and OR ("f(x) + f(y) - f(x)*f(y)") operations. Example equations are defined below in **Equations 1-2**:

Equation 1: Example logic-based differential equation with an AND relationship between C&D => E

$$\frac{dE}{dt} = \frac{1}{\tau_E}(W_{CDE} f_{act}(C) f_{inhib}(D) E_{MAX} - E)$$

Equation 2: Example logic-based differential equation with an OR relationship between A or E => C

$$\frac{dC}{dt} = \frac{1}{\tau_C}\left[\left(W_{AC} f_{act}(A) + W_{EC} f_{act}(E) - W_{AC} f_{act}(A) W_{EC} f_{act}(E)\right) C_{MAX} - C\right]$$

The default node parameters are: $y_{initial} = 0$, $y_{max} = 1$. The default, reaction parameters are: weight = 1, Hill coefficient = 1.4, EC50 = 0.6. The node parameter, tau, is scaled to the type of interaction: 0.1 for enzymatic interaction, 1 for receptor binding, and 10 for protein expression. All parameters outlined above are the same as those used in the original model[1, 10].

Input Levels

Given the importance of fibroblasts in the post-MI wound healing process, we sought to leverage a computational model of fibroblast signaling [1] to model the effect of changes in cytokine and chemokines on fibroblast phenotype. This allows for a uniquely mechanistic study of post-MI signaling. Additionally, the methods described here outline a protocol for utilizing similar computational models to investigate dynamic signaling processes that are difficult to study *in vivo*.

Dynamic levels for all paracrine inputs were defined by curves based on measurements of those inputs in rat hearts post-MI. Measurements were used from rat infarct where available or from rat peri-infarct tissue, whole heart extracts, or cardiac

tissue remote from the infarct as indicated in **Supplementary File 1**. Additionally, we prioritized using measurements of protein levels as the basis of each paracrine signal curve when available, and otherwise mRNA measurements were used.

For each paracrine signal, bi-exponential curves were fit to the post-MI input data. Experimental data of paracrine inputs were first converted to fold-change by normalizing to the first timepoint. Next, we manually fit time constants (p_2 and p_3 from **Equation 3**) to the data. The input curves were then normalized to start at a control normalized level of 0.1 and reach a peak of 0.6 at the time corresponding to the peak signal observed experimentally. This normalization was done by brute force optimization of the magnitude parameter (p_1) to ensure that the peak of the input curves was within 10^{-4} of the indicated peak height.

Due to the uncertainty in defining the peak height, we used an ensemble of paracrine curve sets where the peak height for each individual paracrine curve within a set was randomly sampled from a normal distribution with a mean of 0.6 and a standard deviation of 0.05. Simulations using an ensemble of 500 different paracrine input curve sets were qualitatively similar to simulations performed using paracrine input curve sets where the peak heights were all set to 0.6. For that reason, we show the results of simulations where all peak heights were set to 0.6. Parameters for each input curve are provided in **Table S2**.

Equation 3: Single-peak input equation

$$1 + p_1 e^{-\frac{t}{p_2}}(1 - e^{-\frac{t}{p_3}})$$

Tissue-Level Model

The single-cell signaling model was coupled to a previously reported model of the tissue-level accumulation of collagen (collagen area fraction) [11]. Whereas the tissue-level model previously used a fixed time-dependent curve for collagen mRNA levels, here we drove the model by the collagen I mRNA dynamics predicted by the fibroblast signaling network model. The change in collagen area fraction was modeled based on **Equation 4**. Specifically, the production of collagen is modeled as a product of the collagen generation rate (k_g, 1.92 unit/day), the collagen I mRNA levels (c_n as predicted by the network model), and the number of fibroblasts (n_f). Fibroblast number was based on observed changes in fibroblast proliferation post-MI [12]. The degradation of collagen is the product of the degradation rate (k_d, 0.0243 unit/day), the level of MMP activity (m), and the amount of mature collagen. The k_g and k_d values were optimized to fit the experimental data given the predicted collagen expression from a dynamic simulation with all peak heights set to 0.6, which was considered the standard simulation. The MMP activity level was modeled with **Equation 5**, based on the average of the tissue-level dynamics of MMPs 1, 2, and 9[13].

Equation 4:

$$\frac{dAreaFraction}{dt} = k_g * c_n * n_f - k_d * m * AreaFraction$$

Equation 5:

$$m(t) = kd_1 + kd_2 * e^{(-kd_3 * t)} - e^{(-kd_2 * t)}$$

$$kd_1 = 0.2 \quad kd_2 = 0.5592 \quad kd_3 = 0.10368$$

MATLAB code of the model is freely available on GitHub at: https://github.com/saucermanlab/Zeigler_MIdynamics.

Supplemental References

[1] Zeigler AC, Richardson WJ, Holmes JW, et al. A computational model of cardiac fibroblast signaling predicts context-dependent drivers of myofibroblast differentiation. *J Mol Cell Cardiol*; 94: 72–81.

[2] Cox TR, Bird D, Baker AM, et al. LOX-mediated collagen crosslinking is responsible for fibrosis-enhanced metastasis. *Cancer Res* 2013. Epub ahead of print 2013. DOI: 10.1158/0008-5472.CAN-12-2233.

[3] López B, Querejeta R, González A, et al. Impact of treatment on myocardial lysyl oxidase expression and collagen Cross-linking in patients with heart failure. *Hypertension*; 53: 236–242.

[4] Huet E, Vallée B, Szul D, et al. Extracellular matrix metalloproteinase inducer/CD147 promotes myofibroblast differentiation by inducing α-smooth muscle actin expression and collagen gel contraction: Implications in tissue remodeling. *FASEB J* 2008. Epub ahead of print 2008. DOI: 10.1096/fj.07-8748com.

[5] Hinz B, Celetta G, Tomasek JJ, et al. Alpha-smooth muscle actin expression upregulates fibroblast contractile activity. *Mol Biol Cell* 2001. Epub ahead of print 2001. DOI: 10.1091/mbc.12.9.2730.

[6] Voloshenyuk TG, Landesman ES, Khoutorova E, et al. Induction of cardiac fibroblast lysyl oxidase by TGF-β1 requires PI3K/Akt, Smad3, and MAPK signaling. *Cytokine* 2011. Epub ahead of print 2011. DOI: 10.1016/j.cyto.2011.03.024.

[7] Voloshenyuk TG, Hart AD, Khoutorova E, et al. TNF-?? increases cardiac fibroblast lysyl oxidase expression through TGF-?? and PI3Kinase signaling pathways. *Biochem Biophys Res Commun*; 413: 370–375.

[8] Hall MC, Young DA, Waters JG, et al. The comparative role of activator protein 1 and Smad factors in the regulation of Timp-1 and MMP-1 gene expression by transforming growth factor-β1. *J Biol Chem*; 278: 10304–10313.

[9] Yuan W, Varga J. Transforming growth factor-beta repression of matrix metalloproteinase-1 in dermal fibroblasts involves Smad3. *J Biol Chem*; 276: 38502–10.

[10] Kraeutler MJ, Soltis AR, Saucerman JJ. Modeling cardiac β-adrenergic signaling with normalized-Hill differential equations: comparison with a biochemical model. *BMC Syst Biol*; 4: 157.

[11] Clarke SA, Richardson WJ, Holmes JW. Modifying the mechanics of healing infarcts: Is better the enemy of good? *Journal of Molecular and Cellular Cardiology* 2016. Epub ahead of print 2016. DOI: 10.1016/j.yjmcc.2015.11.028.

[12] Fishbein MC, Maclean D, Maroko PR. The histopathologic evolution of myocardial infarction. *Chest*; 73: 843–849.

[13] Cleutjens JPM, Kandala JC, Guarda E, et al. Regulation of collagen degradation in the rat myocardium after infarction. *J Mol Cell Cardiol* 1995. Epub ahead of print 1995. DOI: 10.1016/S0022-2828(05)82390-9.

Supplemental Files

Supplemental File 1: Experimental data used to determine paracrine input dynamics.

Supplemental Video 1: Network visualization of dynamic post-MI model showing time-dependent activation of each network node in response to the dynamic paracrine input curves.

Supplemental Tables

Table S1: Supporting data for additional reactions in model update

Reaction	Primary source cell type	Primary Source PMID	Secondary source cell type	Secondary Source PMID	Additional PMID
Akt => LOX	rat CF	21498085	rat CF	21893029	
LOX & CI => xlinkFibers	human myocardium	19075089	mouse lung	23345161	
AP1 & !smad3 => proMMP1	human cardiac fibroblast	17921324	human dermal fibroblasts	11502752	12525489
FA => contraction	rat dermal fibroblast, rat lung fibroblast	11553712	human corneal fibroblast	17965264	
aSMA => contraction	rat dermal fibroblast, rat lung fibroblast	11553712	human corneal fibroblast		

Table S2: Parameters for each of the dynamic post-MI paracrine inputs

Input	p1	p2	p3
TGFb	209	1000	50
IL6	6687	10	550
IL1	66	18	6
TNFa	40	1000	50
NE	0.5	3200	750
ET1	90	120	60
BNP	91	120	60
AngII	10	3200	750
PDGF	18	400	560

Supplemental Figures

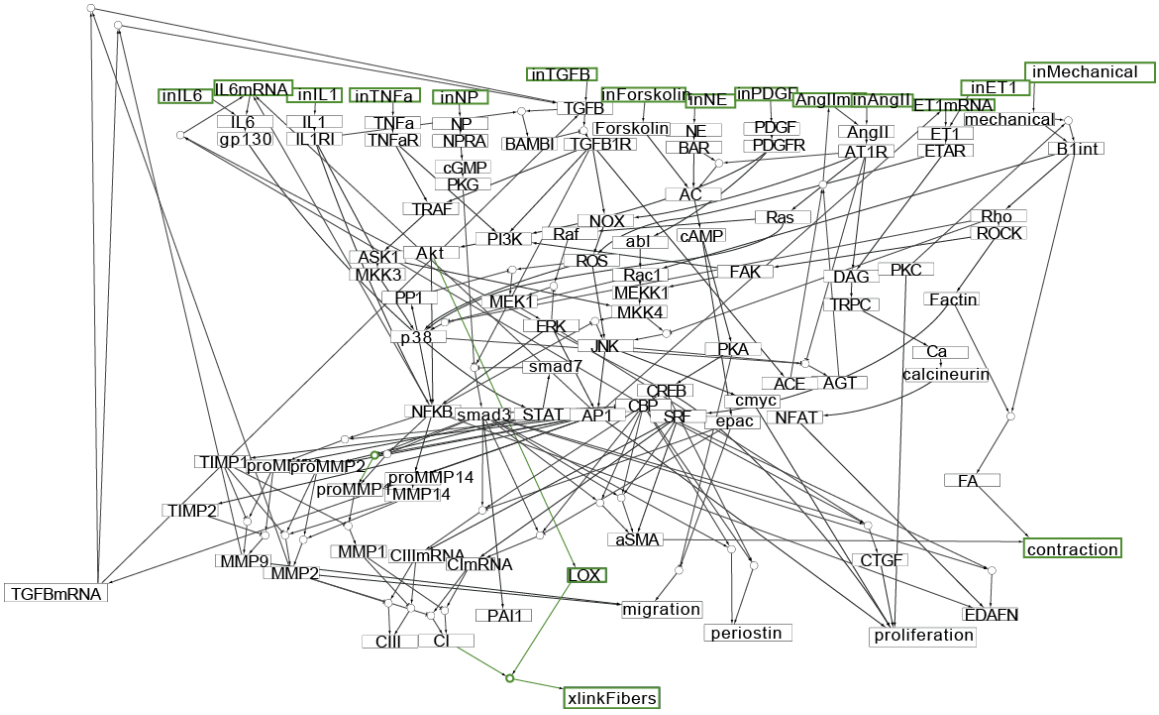

Figure S1: Network Modifications. Network diagram of the fibroblast network model, with additions as described in Supplemental Methods. Green color highlights the interactions and nodes that were added to the network model in this study.

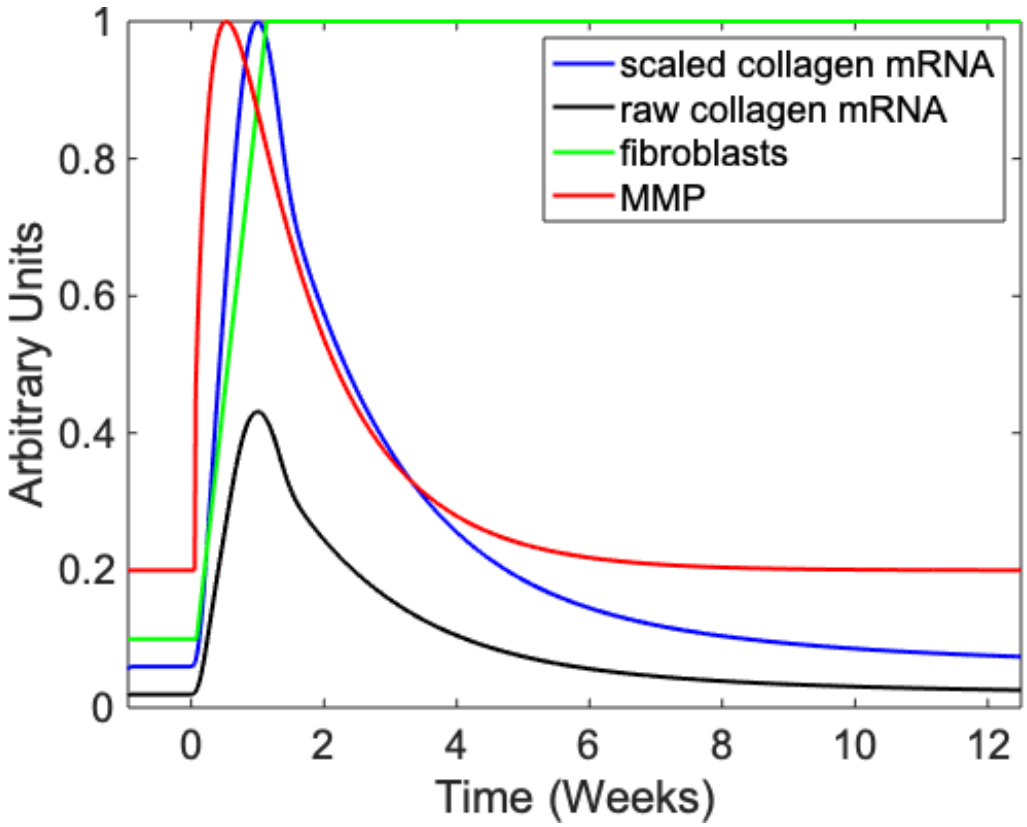

Figure S2: Inputs to tissue-level model for simulations of post-MI wound healing. Fibroblast number and MMP levels are defined by an idealized input curve based on post-MI data as described in Supplementary Methods. Collagen I expression is the collagen I mRNA level predicted by the network model, normalized to a max value of 1.

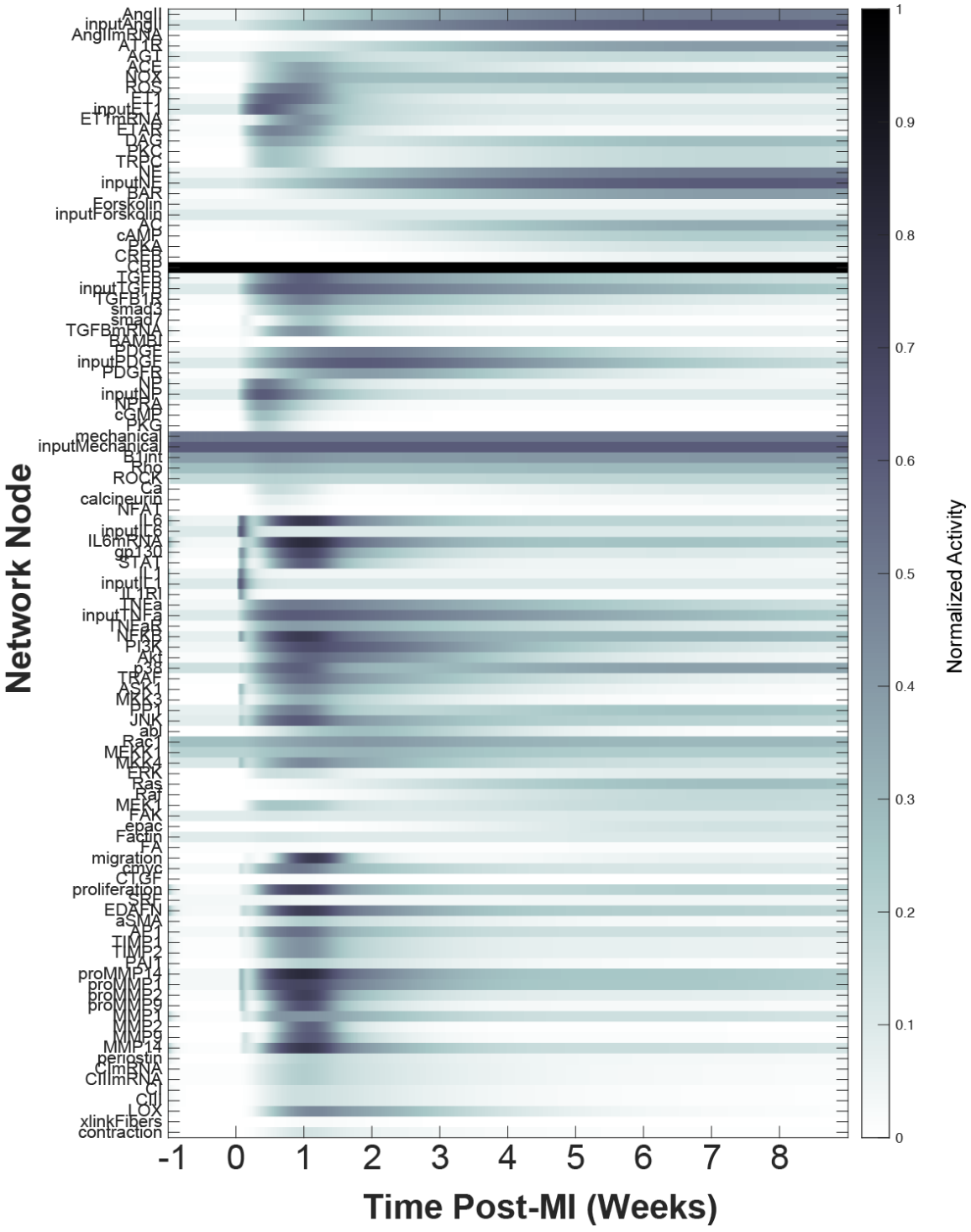

Figure S3: Predicted dynamics of activation of each network node in simulation of the post-MI environment with nine dynamic paracrine stimuli.

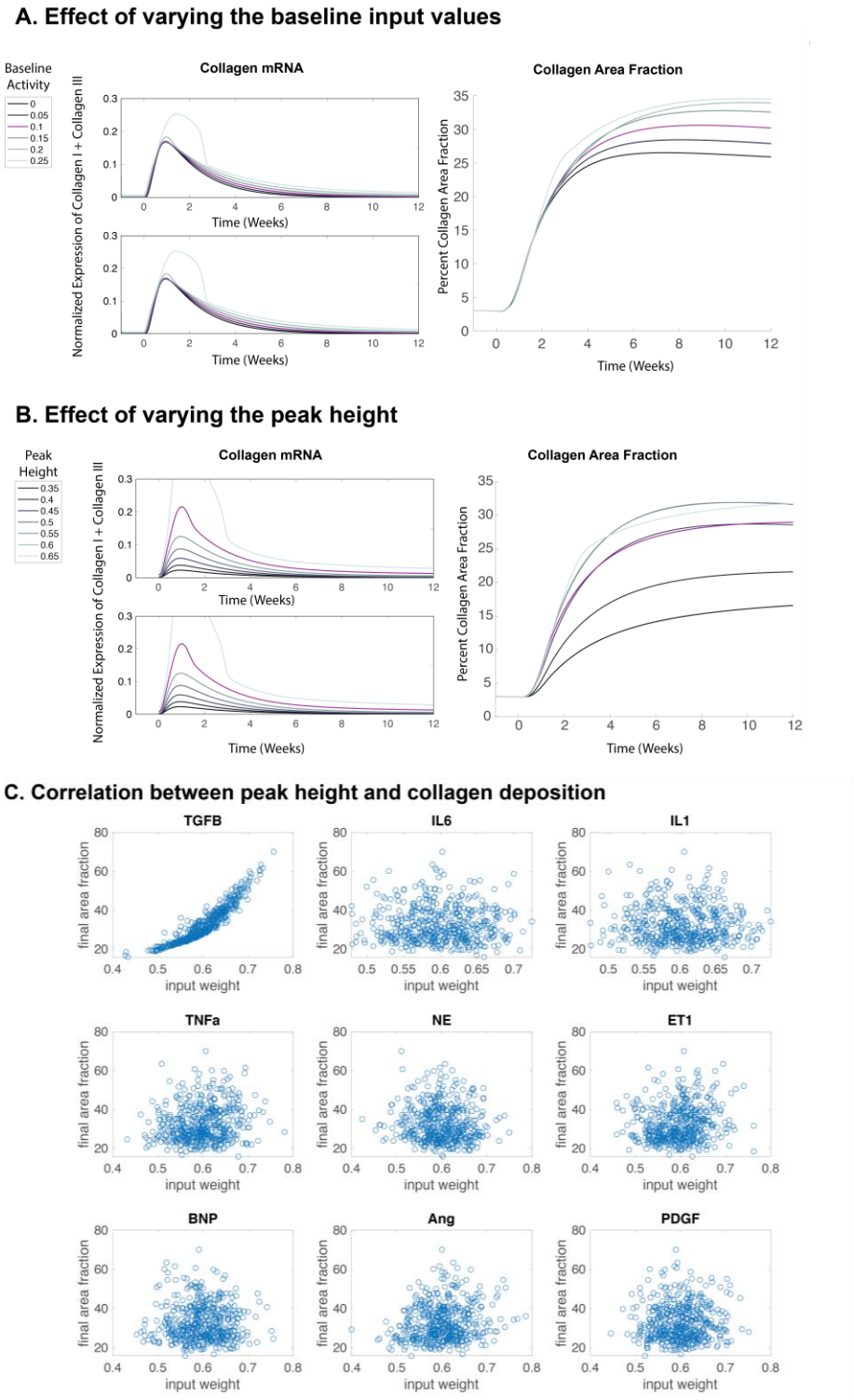

Figure S4: Effect of changing post-MI paracrine baseline and peak height on collagen mRNA and area fraction. Predicted collagen expression and accumulation are shown for paracrine curves sets where the baseline value (A) or peak height (B) for all paracrine curves was varied. C) For the ensemble model where peak heights were randomly sampled from a normal distribution centered around 0.6, the final collagen area fraction at 12 weeks was compared to the peak height of each individual paracrine curve.

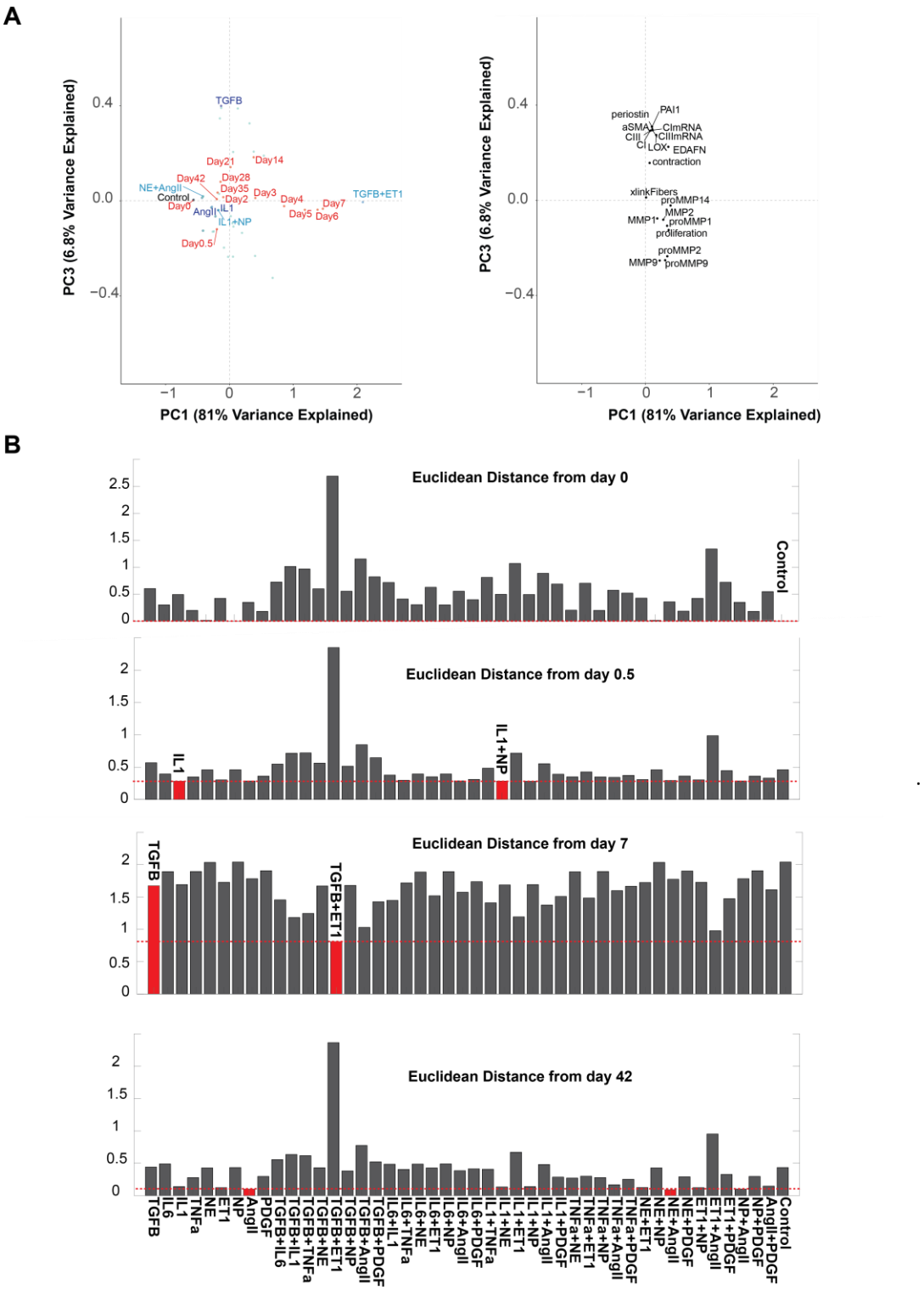

Figure S5: Relationships between dynamic and static paracrine stimuli. A) The dynamic and static stimuli are plotted along the PC1 and PC3 axes, from the same analysis performed in Figure 3. B) The Euclidean distance from each static stimulus to the indicated post-MI timepoint based on the activity of all output nodes is plotted, with the best matching single and paired static paracrine stimuli indicated in red.

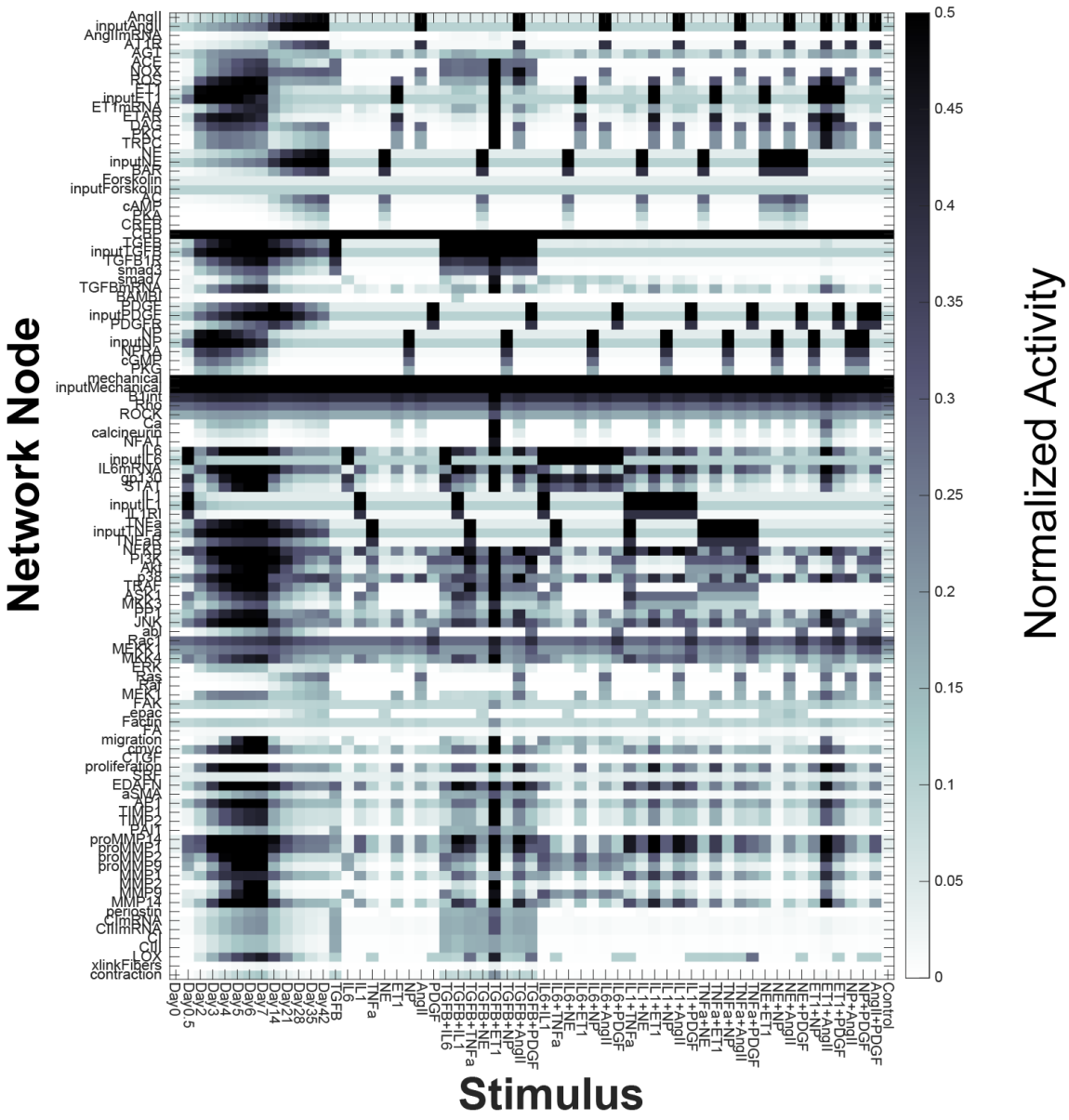

Figure S6: Network-wide activation profiles in response to each single-input and double-input static condition. Each row represents a different node, and each column represents a time point in the dynamic post-MI simulation (Days 0-42) or a static simulation with a single static paracrine stimulus, two static paracrine stimuli, or no stimulus (control).

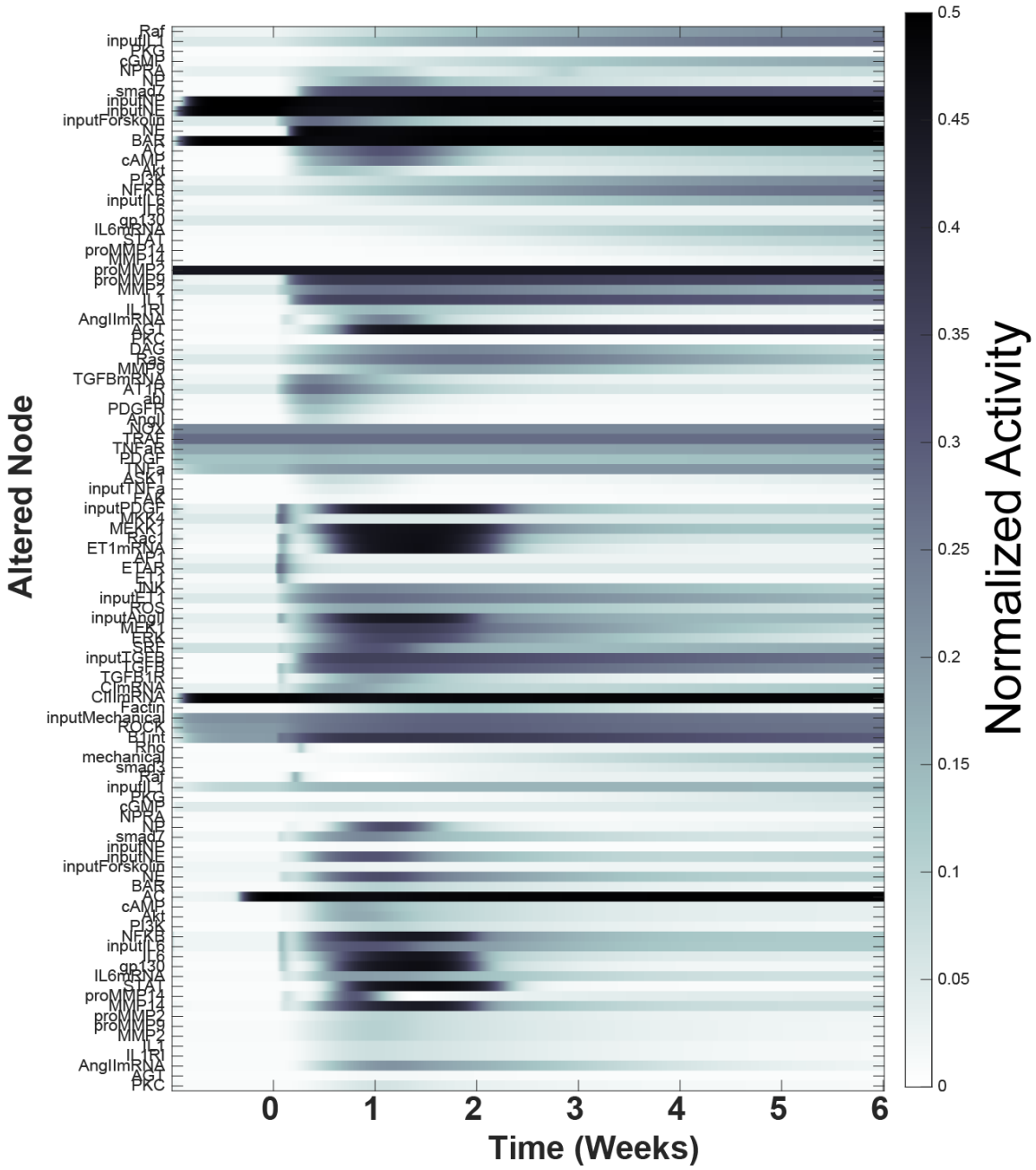

Figure S7: Dynamics of overexpressed nodes from the overexpression screen with dynamic post-MI inputs. As in **Figure 5**, each row represents a simulation in which the nine dynamic paracrine stimuli were used as inputs, with the indicated node increased from ymax = 1 to ymax = 10. Here, the heatmap shows the dynamic activity of that overexpressed node.

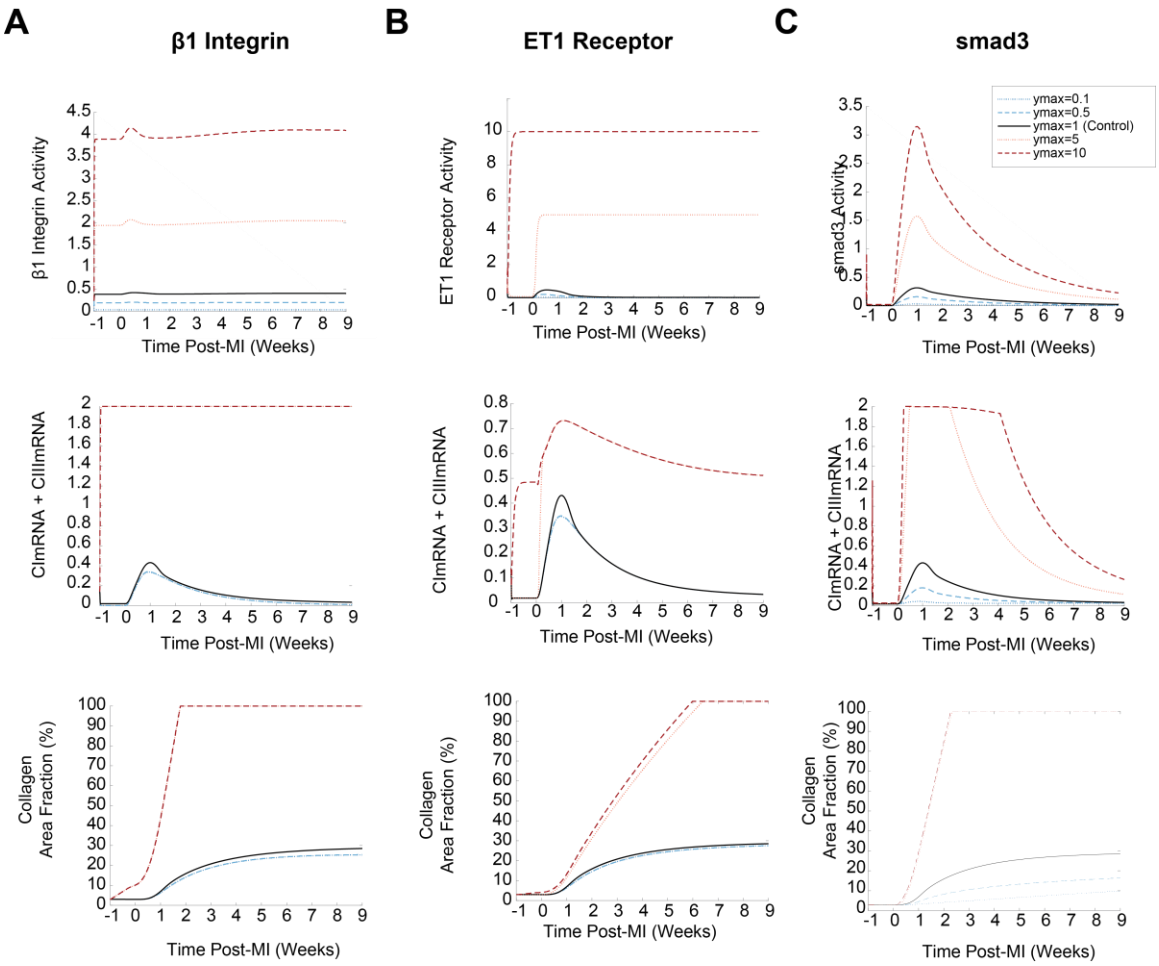

Figure S8: Mechanisms contributing to regulation of collagen expression post-MI with altered expression of A) β1-integrin, B) ET1AR, and C) smad3. As in **Figure 6**, node activity, collagen mRNA expression, and collagen area fraction are shown for control levels of expression (black line, ymax = 1), overexpression (ymax = 5 or 10), or knockdown (ymax = 0.1 or 0.5) of the indicated node.